2001-2022 global gross primary productivity dataset using an ensemble model based on random forest

Xin Chen[1], Tiexi Chen[1,2,3*], Xiaodong Li[4], Yuanfang Chai[5], Shengjie Zhou[1], Renjie Guo[6], Jie Dai[1]

[1]School of Geographical Sciences, Nanjing University of Information Science and Technology, Nanjing 210044, Jiangsu, China.
[2]Qinghai Provincial Key Laboratory of Plateau Climate Change and Corresponding Ecological and Environmental Effects, Qinghai University of Science and Technology, Xining 810016, China
[3]School of Geographical Sciences, Qinghai Normal University, Xining 810008, Qinghai, China.
[4]Qinghai Institute of Meteorological Science, Xining 810008, Qinghai, China.
[5]Department of Earth Sciences, Vrije Universiteit Amsterdam, Boelelaan 1085, 1081 HV, Amsterdam, the Netherlands
[6]Faculty of Geographical Science, Beijing Normal University, Beijing, China.

Correspondence to: Tiexi Chen (txchen@nuist.edu.cn)

Abstract. Advancements in remote sensing technology have significantly contributed to the improvement of models for estimating terrestrial gross primary productivity (GPP). However, discrepancies in the spatial distribution and interannual variability within GPP datasets pose challenges to a comprehensive understanding of the terrestrial carbon cycle. In contrast to previous models that rely on remote sensing and environmental variables, we developed an ensemble model based on the random forest (ERF model). This model used GPP outputs from established models (EC-LUE, GPP-kNDVI, GPP-NIRv, Revised-EC-LUE, VPM, MODIS) as inputs to estimate GPP. The ERF model demonstrated superior performance, explaining 85.1% of the monthly GPP variations at 170 sites, surpassing the performance of selected GPP models (67.7%-77.5%) and an independent random forest model using remote sensing and environmental variables (81.5%). Additionally, the ERF model improved accuracy across each month and various subvalues, mitigating the issue of "high value underestimation and low value overestimation" in GPP estimates. Over the period from 2001 to 2022, the global GPP estimated by the ERF model was 132.7 PgC yr^{-1}, with an increasing trend of 0.42 PgC yr^{-2}, which ~~is~~ was comparable to or slightly better than the accuracy of other mainstream GPP datasets in term of validation results of GPP observations independent of FLUXNET (ChinaFlux). Importantly, for the growing number of GPP datasets, our study provides a way to integrate these GPP datasets, which may lead to a more reliable estimate of global GPP.

1 Introduction

Gross primary productivity (GPP) is the largest carbon flux in the global carbon cycle, and serves as the primary input of carbon into the terrestrial carbon cycle. Uncertainties in GPP estimates can propagate to other carbon flux estimates, making it crucial to clarify the spatio-temporal patterns of GPP (Ruehr et al., 2023; Xiao et al., 2019). However, global GPP is variously estimated from 90 PgC yr^{-1} to 160 PgC yr^{-1} across different studies, with these variations becoming more pronounced when scaled down to regional scales or specific ecosystem types (Anav et al., 2015; Jung et al., 2020; Ryu et al., 2019). This variability underscores the necessity for innovative methods to reduce uncertainty in GPP estimates.

The light use efficiency (LUE) model is one of the most widely adopted methods for estimating GPP. It assumes that GPP is proportional to the photosynthetically active radiation absorbed by vegetation, and optimizes the spatio-temporal pattern of GPP through meteorological constraints such as temperature and moisture (Pei et al., 2022). However, variations in these constraints varies significantly, leading to differences of over 10% in model explanatory power. (Yuan et al., 2014). Recent studies have proposed some novel vegetation indices that have been shown to be effective proxies for GPP through theoretical derivation and observed validation (Badgley et al., 2017; Camps-Valls et al., 2021). However, these vegetation indices often use only remote sensing data as an input for estimating long-term GPP without considering meteorological factors, which has led to some controversy (Chen et al., 2024; Dechant et al., 2022; Dechant et al., 2020). Both LUE and vegetation index models use linear mathematical formulas to estimate GPP, but ecosystems are inherently complex, and the biases introduced by these numerical models increase the uncertainty of GPP estimates. Machine learning models have shown great potential for improving GPP estimates in previous studies (Guo et al., 2023; Jung et al., 2020). These models are trained by non-physical means directly using GPP observations and selected environmental and vegetation variables, and the performance of the models depends on the number and quality of observed data and the representativeness of input data. Nevertheless, direct validation from flux towers of FLUXNET reveals that these models typically explain only about 70% of monthly GPP variations, with similar performance to other GPP estimate models (Badgley et al., 2019; Jung et al., 2020; Wang et al., 2021; Zheng et al., 2020). Due to deviations in the model structure, a common limitation across these models is the poor estimate of monthly extreme GPP, leading to the phenomenon of "high value underestimation~~overestimation~~ and low value overestimation" (Zheng et al., 2020). Especially for extremely high values, which usually occur during the growing season and largely determine the annual totals and interannual fluctuations of GPP, this underestimation may hinder our understanding of the global carbon cycle.

It is challenging for a single model to provide accurate estimates for all global regions. ~~Ensemble models have outperformed individual models in previous studies, potentially addressing some inherent issues in model estimate~~Previous studies have shown that ensemble models perform significantly better than single models and can handle some inherent issues in single models (Chen et al., 2020; Yao et al., 2014). Traditional multi-model ensemble methods usually use a simple multi-model average or a weighted Bayesian average. However, these methods typically assign fixed weights to each model and are essentially linear combinations. Recent studies have incorporated machine learning techniques to multi-model ensembles to establish nonlinear relationships between multiple simulated target variables and real target variable, improving simulation performance (Bai et al., 2021; Tian et al., 2023; Yao et al., 2017). Whether this method can improve some common problems with individual GPP estimate models, such as high value underestimation and low value overestimation, is not clear and needs to further investigation.

In this study, we attempt to use an ensemble model based on the random forest (ERF model) to improve global GPP estimate. Specifically, the work of this study includes the following: (1) Recalibrating parameters for each model, and comparing the performance of six GPP estimate models and the ERF model; (2) Focusing on the phenomenon of "high value underestimation and low value overestimation" in each model, and evaluating the performance of each model across different months, vegetation types and subvalues (high value, median value, low value); (3) Developing a global GPP dataset using the ERF model and validating its generalization using GPP observations from ChinaFlux.

2 Method

2.1 Data at the global scale

In this study, we selected remote sensing data from the Moderate Resolution Imaging Spectroradiometer (MODIS) and meteorological data from EAR5 to estimate global GPP (Hersbach et al., 2020). For the remote sensing data, surface reflectance (red band, near infrared band, blue band and shortwave infrared band), leaf area index (LAI) and fraction of photosynthetically active radiation (FPAR) were used. For meteorological data, we selected average air temperature, dew point temperature, minimum air temperature, total solar radiation and direct solar radiation. Dew point temperature and average air temperature were used to calculate saturated vapor pressure difference (VPD) (Yuan et al., 2019), and diffuse solar radiation (DifSR) was derived as the difference between total solar radiation and direct solar radiation. Minimum air temperature was obtained from the hourly air temperature. CO_2 data were obtained from the monthly average carbon dioxide levels measured by the Mauna Loa Observatory in Hawaii. Table 1 provides an overview of the datasets used in this study.

Table 1. Overview of the datasets used in this study.

Variable	Dataset	Spatial resolution	Temporal resolution	Temporal coverage
Surface reflectance (red band and near infrared band)	MCD43C4	0.05 °	daily	2001-2022
Surface reflectance (red band, near infrared band, blue band and shortwave infrared band)	MOD09CMG	0.05 °	daily	2001-2022
LAI	MOD15A2H	500m	8d	2001-2022
FPAR	MOD15A2H	500m	8d	2001-2022

Average air temperature (AT)	ERA5-land	0.1 °	Monthly	2001-2022
Dew point temperature (DPT)	ERA5-land	0.1 °	Monthly	2001-2022
Minimum air temperature (MINT)	ERA5-land	0.1 °	Monthly	2001-2022
Total solar radiation (TSR)	ERA5 monthly data on single levels	0.25 °	Monthly	2001-2022
Direct solar radiation (DirSR)	ERA5 monthly data on single levels	0.25 °	Monthly	2001-2022
CO_2	NOAA's Earth System Research Laboratory	/	Monthly	2001-2022
Distribution map of C4 crops	Harvested Area and Yield for 175 Crops	1/12 °	Annual	2000
Land use	MCD12C1	0.05 °	Annual	2010

Previous studies have shown that the photosynthetic capacity of C4 crops is much higher than that of C3 crops (Chen et al., 2014; Chen et al., 2011), so it is necessary to divide the cropland into C3 crops and C4 crops. To estimate the global GPP, we used the "175 Crop harvested Area and yield" dataset, which describes the global harvested area and yield of 175 crops in 2000 (Monfreda et al., 2008). We extracted the sum of the area ratios of all C4 crops (corn, corn feed, sorghum, sorghum feed, sugarcane, millet) at each grid as the coverage of C4 crops (Figure S1). Consequently, the estimated value of cropland GPP can be expressed as: coverage of C3 crops × simulated GPP value of C3 crops + coverage of C4 crops × simulated GPP value of C4 crops, which has been used in a previous study (Guo et al., 2023).

The land use map was derived from the IGBP classification of MCD12C1, and 2010 was chosen as the reference year (that is, land use data is unchanged in the simulation of global GPP). In order to meet the requirements of subsequent research, land cover types were grouped into 9 categories: Deciduous Broadleaf Forest (DBF), Evergreen Needleleaved Forest (ENF), Evergreen Broadleaf Forest (EBF), Mixed Forest (MF), Grassland (GRA), Cropland (including CRO-C3 and CRO-C4), Savannah (SAV), Shrub (SHR), Wetland (WET).

Finally, for higher resolution data, we gridded the dataset to 0.05 ° by averaging all pixels whose center fell within each 0.05 ° grid cell for upscaling. For lower resolution data, we used the nearest neighbor resampling method to 0.05 °. In addition, MODIS data were aggregated to a monthly scale to ensure spatio-temporal consistency.

2.2 Observation data at the site scale

GPP observations were sourced from the FLUXNET 2015 dataset, which includes carbon fluxes and meteorological variables from more than 200 flux sites around the world (Pastorello et al., 2020). GPP cannot be obtained directly from flux sites and usually needs to be obtained by dismantling the Net Ecosystem Exchange. We chose a monthly level GPP based on the nighttime partitioning method and retained only high quality data (NEE_VUT_REF_QC > 0.8) for every year, ultimately selecting 170 sites with 10932 monthly values for this study. In addition, we selected monthly average air temperature, total solar radiation and VPD. The site observations do not provide direct solar radiation, so we extracted data from ERA5 covering the flux tower. Monthly minimum air temperature was derived from hourly air temperature. Since some required model data are not directly available at flux sites, LAI and FPAR were extracted from MOD15A2H (500 m), and surface reflectance data (red band, near infrared band, blue band and shortwave infrared band) were derived from MCD43A4 (500 m) and MOD09A1 (500 m). These data are roughly similar to the footprint of the flux site and can represent the land surface of the site (Chu et al., 2021).

2.3 GPP estimate model

We selected six independent models to estimate GPP in this study. These models are widely used with few model parameters and have demonstrated reliable accuracy in previous studies (Badgley et al., 2017; Zhang et al., 2017; Zheng et al., 2020). The six models are EC-LUE, Revised-EC-LUE, NIRv-based linear model, kNDVI-based linear model, VPM, MODIS. The VPM, MODIS and EC-LUE are LUE models based on remote sensing data and meteorological data (Running et al., 2004; Xiao et al., 2004; Yuan et al., 2007). Zheng et al., (2020) proposed the Revised-EC-LUE model, which divides the canopy into sunlit and shaded leaves, improving the estimate of global GPP (Zheng et al., 2020). The NIRv and kNDVI are novel vegetation indices calculated from the red and near-infrared bands of the reflectance spectrum (Badgley et al., 2017; Camps-Valls et al., 2021). Similar to solar induced chlorophyll fluorescence, they exhibit a linear relationship with GPP and are considered effective proxies for GPP. Detailed descriptions of all models can be found in Text S1.

To reduce uncertainty in GPP estimates from a single model, we used the ERF model, the basic idea of which is to restructure the simulated values of multiple models. In this study, we directly used the ERF model to establish the relationship between the GPP simulated by the above six models and GPP observations. In addition, for comparison with the ERF model, we also used the random forest (RF) method for modeling. In this study, we used average air temperature, minimum air temperature, VPD, direct solar radiation, diffuse solar radiation, FPAR and LAI as explanatory variables.~~to estimate GPP.~~ Both models used the random forest method, which has been widely used in previous studies of GPP estimate (Guo et al., 2023; Jung et al., 2020). Random forest is an ensemble learning algorithm that combines the outputs of multiple decision trees to produce a single result, and is commonly used for classification and regression problems (Belgiu and Drăguţ, 2016). In the regression problem, the output result of each decision tree is a continuous value, and the average of all decision tree outputs is taken as the final result. An overview of all models used can be found in Table 2.

Table 2. Overview of the models used in this study.

ID	Model	Input data	Output
1	EC-LUE	FPAR, VPD, AT, SRAD, CO_2	GPP_{EC}
2	Revised-EC-LUE	LAI, VPD, AT, DifSR, DirSR, CO_2	GPP_{REC}
3	kNDVI-GPP	Red band and near infrared band (MCD43)	GPP_{kNDVI}
4	NIRv-GPP	Red band and near infrared band (MCD43)	GPP_{NIRv}
5	VPM	Red band, near infrared band, blue band, shortwave infrared band (MOD09), AT, SRAD	GPP_{VPM}
6	MODIS	FPAR, SRAD, MINT, VPD	GPP_{MODIS}
7	Random forest model (RF)	LAI, FPAR, AT, MINT, VPD, DifSR, DirSR	GPP_{RF}
8	Ensemble model based on random forest (ERF)	GPP_{EC}, GPP_{REC}, GPP_{kNDVI}, GPP_{NIRv}, GPP_{MODIS}, GPP_{VPM}	GPP_{ERF}

2.4 Model parameter calibration and validation

FLUXNET only provides GPP observations and meteorological data, lacking direct measurements for LAI, FPAR, and surface reflectance, so remote sensing data is needed. Considering the variety of remote sensing data sources, such as MODIS and AVHRR, it is evident that calibrating the same GPP estimate model with different remote sensing data can yield varied parameters. In addition, the number of sites used to calibrate model parameters is also an important influencing factor for model parameters. The original parameters of these models were calibrated with only a limited number of sites (e.g., 95 sites for Revised EC-LUE and 104 for NIRv-GPP) (Wang et al., 2021; Zheng et al., 2020). Therefore, to reduce the impact of the uncertainty of model parameters on simulation results, we did not use original parameters and conducted parameter calibration for GPP estimate models across different vegetation types. For EC-LUE, Revised EC-LUE, VPM and MODIS, the Markov chain Monte Carlo method was used to calibrate model parameters. Traditionally, the mean of the posterior distribution of parameters is taken as the optimal value. However, previous studies have indicated that some model parameters are not well constrained when calibrating multiple model parameters (Wang et al., 2017; Xu et al., 2006), so we selected the parameter with the smallest root-mean-square error (RMSE) as the optimal parameter in each iteration. For each vegetation type, we randomly selected 70% of the ~~sites~~ data for parameter calibration, and repeated the process 200 times. In order to avoid overfitting, we adopted the mean of the 200 calibrated parameters as the final model parameters. Similarly, for the two vegetation index models, we randomly selected 70% of the data~~sites~~ in each vegetation type for parameter calibration, repeating the process 200 times and using the mean of the 200 calibrated parameters as the final model parameters.

After obtaining GPP estimates from the six GPP models, we evaluated the simulation performance of the RF model and the ERF model respectively. For both models, we evaluated the model performance using 5-fold cross-validation, where the process was repeated 200 times, and the mean of the 200 GPP estimates was considered the final GPP estimate. In addition, we used a second validation method~~,~~ in which all data from 70% of the sites were selected for modeling and only all data from the remaining 30% of the sites were validated, a process that was repeated 200 times. This validation will further illustrate the generalization of the model, i.e. its potential for estimating ~~sites~~GPP without~~ GPP~~ observations.~~In addition, we used a second validation method where 70% of the data was selected for modeling and only the remaining 30% was validated, a process that was repeated 200 times.~~ We utilized the determination coefficient (R^2) and RMSE as metrics to evaluate the simulation performance of all models. Additionally, we used the ratio of GPP simulations to GPP observations (Sim/Obs) to measure whether the model overestimates or underestimates.

2.5 Global GPP estimate based on ERF model and its uncertainty.

Based on the ERF model, we estimated global GPP for 2001-2022 (ERF_GPP). It is important to note that in this process, we used all the site data to build the model. The uncertainties of ERF_GPP can be attributed to two primary factors: the influence of the number of GPP observations and the influence of the number of features (that is, the simulated GPP). For the first type of uncertainty, we randomly selected 80% of the data to build a model and simulated the multi-year average of global GPP. The process was repeated 100 times, yielding 100 sets of multi-year averages of ERF_GPP. Their standard deviations were considered as the uncertainty of ERF_GPP caused by the number of GPP observations. For the second type of uncertainty, we selected different number of features to build a model and simulated the multi-year average of global GPP. A total of 56 sets of multi-year averages of ERF_GPP were obtained. The standard deviation of different combinations was considered to be the uncertainty of ERF_GPP caused by the number of features.

2.6 Evaluation of the generalization of different GPP datasets

The majority of flux sites in FLUXNET are concentrated in Europe and North America, it is unclear whether the different GPP estimate methods are suitable for regions with sparse flux sites. Recently, ChinaFlux has published GPP observations from several sites, offering an opportunity to evaluate the generalization of different GPP datasets. However, the spatial resolution of most GPP datasets is 0.05°, and a direct comparison with GPP observations at flux sites is challenging. Therefore, we extracted 0.05° MODIS land use covering the flux sites. If the vegetation type of the flux site matched the MODIS land use, the site was used for the analysis. Finally, a total of 12 flux sites were selected (Figure S2), and Table S1 shows the information of these sites. The same procedure was applied to FLUXNET, resulting in the selection of 52 sites (Figure S2). It should be noted that due to the absence of meteorological data from some sites in Chinaflux, we did not validate all GPP estimate models at the site scale (500 m).

We evaluated the generalization of ERF_GPP at 12 ChinaFlux sites and 52 FLUXNET sites. In addition, we selected a number of widely used GPP datasets for comparison, including BESS (Li et al., 2023), GOSIF (Li and Xiao, 2019), FLUXCOM: random forest-based version (FLUXCOM-RF) and ensemble version (FLUXCOM-ENS) (Jung et al., 2020), NIRv (Wang et al., 2021), Revise-EC-LUE (Zheng et al., 2020), MODIS (Running et al., 2004), VPM (Zhang et al., 2017), which were generated using different GPP estimate methods. These GPP datasets all have a spatial resolution of 500 m-0.5 °, similar to the resampling process in section 2.1, we have unified them to 0.05 °. The common time range for these datasets spanned from 2001 to 2018, and the temporal resolution was unified to monthly to match the GPP observations.

3 Result

3.1 Performance of GPP estimate models at site scale

Table S2-S7 show the optimization results of the six GPP estimate model parameters. Consistent with previous study, in the Revised EC-LUE model, the light use efficiency parameter of shade leaves was significantly higher than that of sunlit leaves (Zheng et al., 2020). It is necessary to divide cropland into C3 crops and C4 crops. In all models, the light use efficiency parameters of C4 crops were significantly higher than those of C3 crops, which was particularly reflected in the two vegetation index models of GPP_{kNDVI} and GPP_{NIRv}, the slope of the linear regression directly reflected the difference in photosynthetic capacity of the different crops.

Figure 1 shows the performance of all models across different vegetation types. Overall, the performance of the ERF model was better than that of the other GPP estimate models. GPP_{ERF} had the higher accuracy among all models, with R^2 between 0.61-0.91 and RMSE between 0.72-2.78 gC m^{-2} d^{-1}. In contrast, the LUE and vegetation index models performed slightly weaker, especially in EBF, where R^2 was both below 0.5. It is worth noting that compared to other vegetation types, the RMSE was highest for cropland, with 6 out of 8 models for C4 crops exceeding 3 gC m^{-2} d^{-1}, suggesting that these existing GPP estimate models may not properly capture the seasonal changes in cropland GPP. The six models with ~~calibration~~ calibrated parameters and ERF model were found to have no significant deviation across vegetation types. However, GPP_{RF} was significantly underestimated for C4 crops and overestimated for SHR.

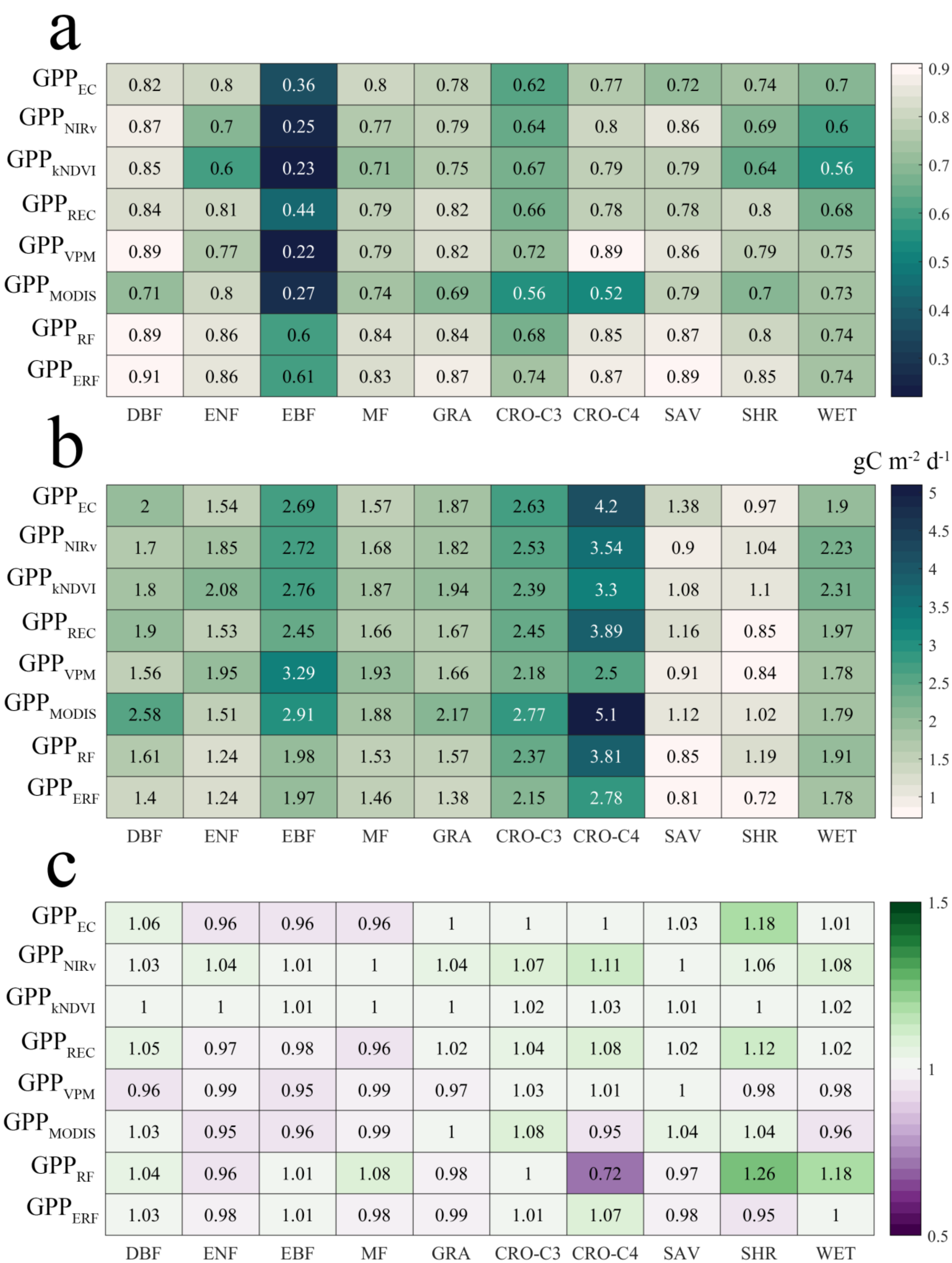
a
GPP_EC 0.82 0.8 0.36 0.8 0.78 0.62 0.77 0.72 0.74 0.7
GPP_NIRv 0.87 0.7 0.25 0.77 0.79 0.64 0.8 0.86 0.69 0.6
GPP_kNDVI 0.85 0.6 0.23 0.71 0.75 0.67 0.79 0.79 0.64 0.56
GPP_REC 0.84 0.81 0.44 0.79 0.82 0.66 0.78 0.78 0.8 0.68
GPP_VPM 0.89 0.77 0.22 0.79 0.82 0.72 0.89 0.86 0.79 0.75
GPP_MODIS 0.71 0.8 0.27 0.74 0.69 0.56 0.52 0.79 0.7 0.73
GPP_RF 0.89 0.86 0.6 0.84 0.84 0.68 0.85 0.87 0.8 0.74
GPP_ERF 0.91 0.86 0.61 0.83 0.87 0.74 0.87 0.89 0.85 0.74
DBF ENF EBF MF GRA CRO-C3 CRO-C4 SAV SHR WET
0.9 0.8 0.7 0.6 0.5 0.4 0.3
b
gC m-2 d-1
GPP_EC 2 1.54 2.69 1.57 1.87 2.63 4.2 1.38 0.97 1.9
GPP_NIRv 1.7 1.85 2.72 1.68 1.82 2.53 3.54 0.9 1.04 2.23
GPP_kNDVI 1.8 2.08 2.76 1.87 1.94 2.39 3.3 1.08 1.1 2.31
GPP_REC 1.9 1.53 2.45 1.66 1.67 2.45 3.89 1.16 0.85 1.97
GPP_VPM 1.56 1.95 3.29 1.93 1.66 2.18 2.5 0.91 0.84 1.78
GPP_MODIS 2.58 1.51 2.91 1.88 2.17 2.77 5.1 1.12 1.02 1.79
GPP_RF 1.61 1.24 1.98 1.53 1.57 2.37 3.81 0.85 1.19 1.91
GPP_ERF 1.4 1.24 1.97 1.46 1.38 2.15 2.78 0.81 0.72 1.78
DBF ENF EBF MF GRA CRO-C3 CRO-C4 SAV SHR WET
5 4.5 4 3.5 3 2.5 2 1.5 1
c
GPP_EC 1.06 0.96 0.96 0.96 1 1 1 1.03 1.18 1.01
GPP_NIRv 1.03 1.04 1.01 1 1.04 1.07 1.11 1 1.06 1.08
GPP_kNDVI 1 1 1.01 1 1 1.02 1.03 1.01 1 1.02
GPP_REC 1.05 0.97 0.98 0.96 1.02 1.04 1.08 1.02 1.12 1.02
GPP_VPM 0.96 0.99 0.95 0.99 0.97 1.03 1.01 1 0.98 0.98
GPP_MODIS 1.03 0.95 0.96 0.99 1 1.08 0.95 1.04 1.04 0.96
GPP_RF 1.04 0.96 1.01 1.08 0.98 1 0.72 0.97 1.26 1.18
GPP_ERF 1.03 0.98 1.01 0.98 0.99 1.01 1.07 0.98 0.95 1
DBF ENF EBF MF GRA CRO-C3 CRO-C4 SAV SHR WET
1.5 1 0.5

Figure 1. The performance of the eight models on different vegetation types. a, b and c represent R^2, RMSE, and Sim/Obs respectively.

Combining the results of all flux sites, GPP_{ERF} explained 85.1% of the monthly GPP variations, while the seven GPP estimate models only explained 67.7%-81.5% of the monthly GPP variations (Figure 2). Another validation method also showed similar results, the average R^2 and RMSE of 200 validation results of ERF model were 0.822 and 1.68 gC m-2 d^{-1}, which were obviously better than other models ~~Another validation method also showed similar results~~ (Figure S3). In order to further prove the robustness of the ERF model, we also used GPP estimate models with original parameters for modeling and validation. As shown in Figure S4, the performance of these GPP models decreased significantly, with R^2 ranging from 0.570 to 0.719 and RMSE ranging from 2.29 to 3.81 gC m^{-2} d^{-1}. The phenomenon of "high value underestimation and low value overestimation" was also pronounced. However, the ERF model maintained a consistent advantage, with R^2 significantly higher than other GPP estimate models (0.856). In addition, we tested the effect of the number of GPP estimate models on the accuracy of the ERF model. As shown in Table S8, as the number of GPP in the ERF model increased, the performance gain of the model gradually decreased.

In summary, GPP_{ERF} showed high accuracy in terms of vegetation type and the ability to interpret monthly variations in GPP, which also illustrates the potential of the ERF model to improve GPP estimate. However, it was observed that most GPP simulations exhibited the phenomenon of “high value underestimation and low value overestimation”. For example, GPP_{EC}, GPP_{REC}, GPP_{MODIS} and GPP_{RF} showed obvious underestimation in the months when the monthly GPP value surpassed 15 gC m^{-2} d^{-1} (Figure 2). Therefore, it is necessary to evaluate the performance of different models in each month and different subvalues.

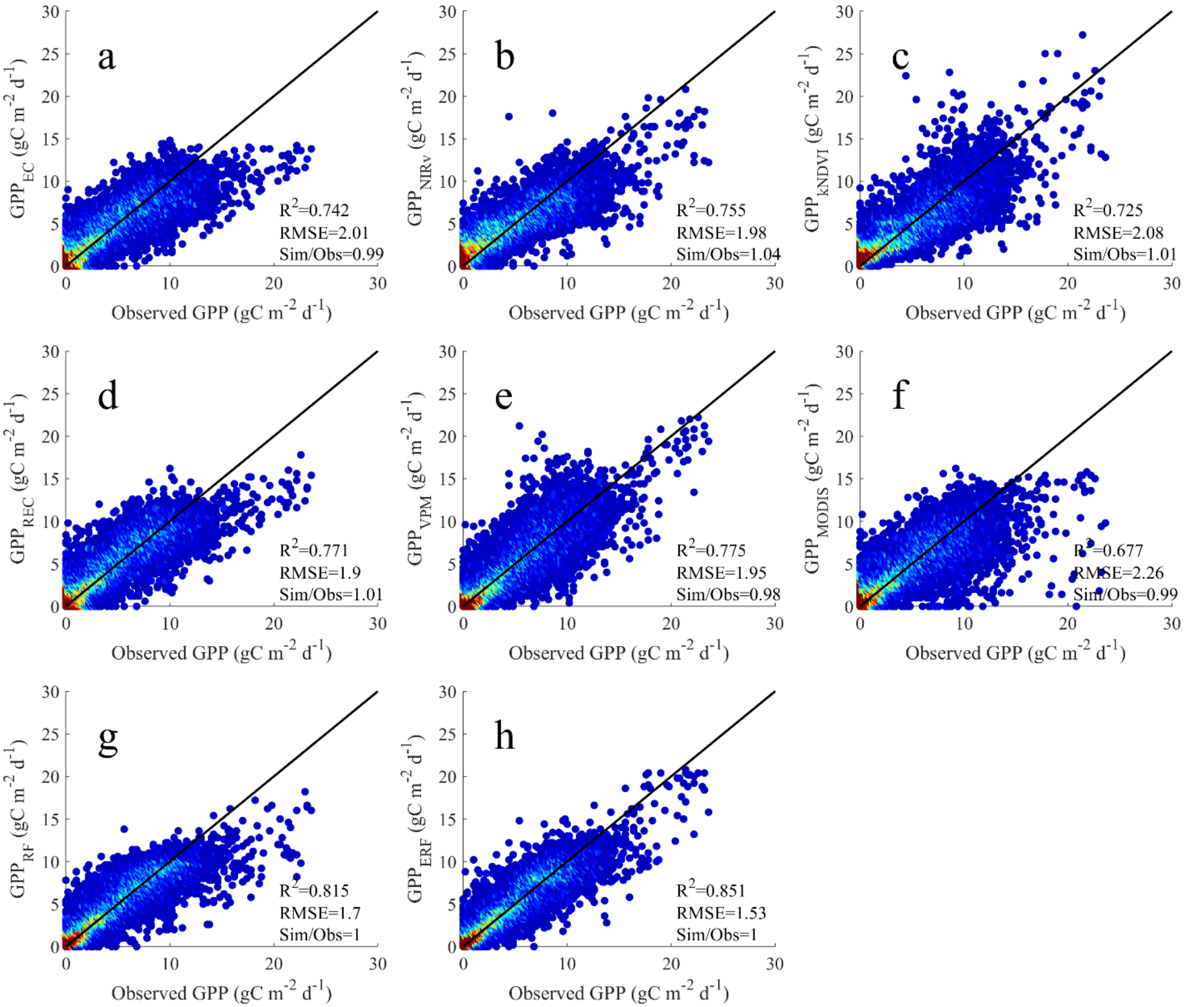

Figure 2. Comparison between the GPP simulations of the eight models and the GPP observations. a-h represents GPP_{EC}, GPP_{NIRv}, GPP_{kNDVI}, GPP_{REC}, GPP_{VPM}, GPP_{MODIS}, GPP_{RF}, GPP_{ERF}, respectively.

3.2 Performance of GPP estimate models in each month and different subvalues

Figure 3 shows the simulation accuracy of the eight models in each month. The ERF model maintained a higher accuracy than other GPP estimate models, with GPP_{ERF} consistently achieving higher R^2 and lower RMSE in most months, and no evident phenomenons of "high value underestimation and low value overestimation". In contrast, the accuracy of other GPP estimate models was less satisfactory accuracy, especially during winter (most flux sites are concentrated in the Northern Hemisphere), the LUE models tended to underestimate GPP, and the Sim/Obs remained at 0.72-1.01, although R^2 were above 0.7. Meanwhile, the vegetation index models overestimated GPP, Sim/Obs remained at 1.34-1.73, and R^2 were relatively low, mostly around 0.6.

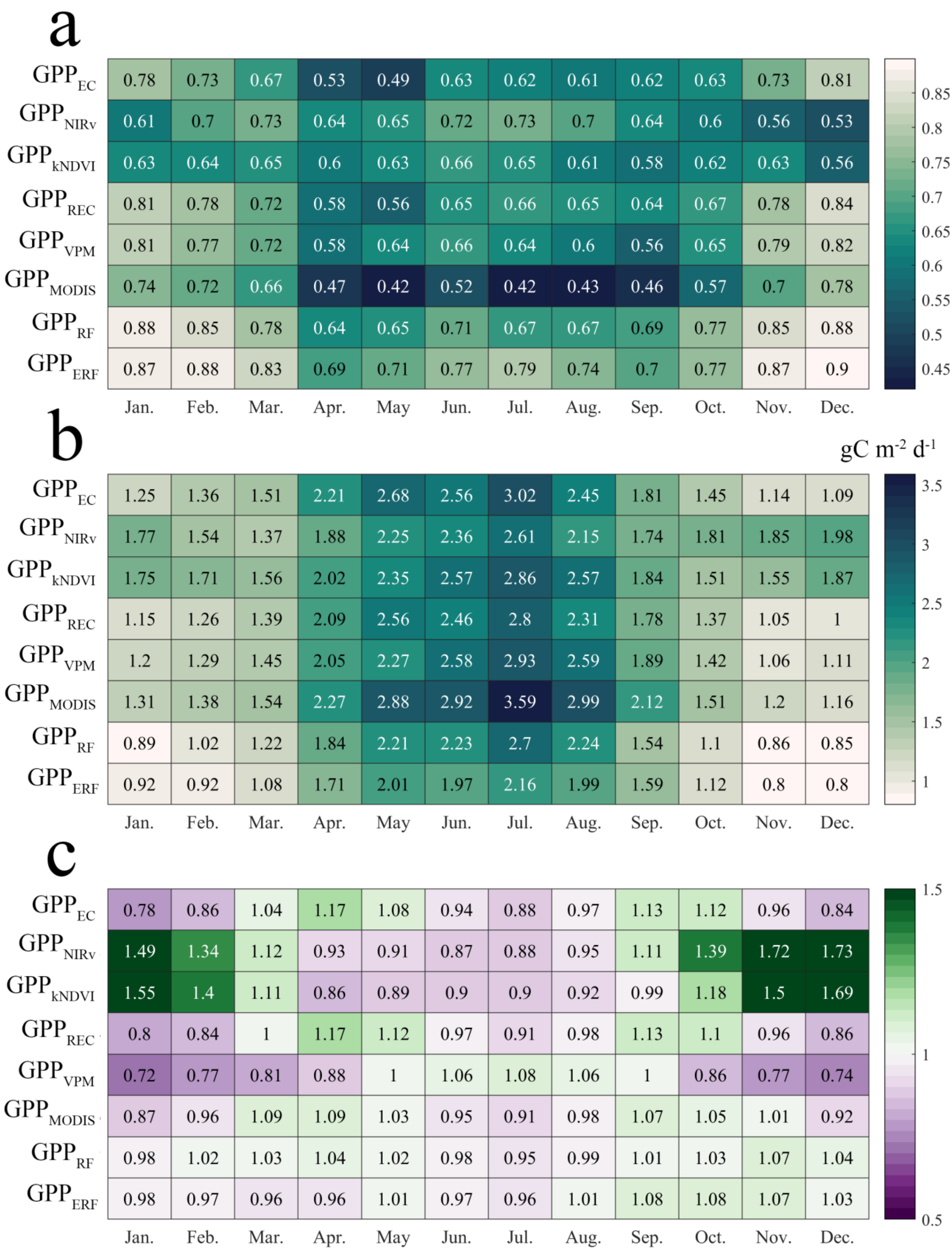
a
GPP EC 0.78 0.73 0.67 0.53 0.49 0.63 0.62 0.61 0.62 0.63 0.73 0.81
GPP NIRv 0.61 0.7 0.73 0.64 0.65 0.72 0.73 0.7 0.64 0.6 0.56 0.53
GPP kNDVI 0.63 0.64 0.65 0.6 0.63 0.66 0.65 0.61 0.58 0.62 0.63 0.56
GPP REC 0.81 0.78 0.72 0.58 0.56 0.65 0.66 0.65 0.64 0.67 0.78 0.84
GPP VPM 0.81 0.77 0.72 0.58 0.64 0.66 0.64 0.6 0.56 0.65 0.79 0.82
GPP MODIS 0.74 0.72 0.66 0.47 0.42 0.52 0.42 0.43 0.46 0.57 0.7 0.78
GPP RF 0.88 0.85 0.78 0.64 0.65 0.71 0.67 0.67 0.69 0.77 0.85 0.88
GPP ERF 0.87 0.88 0.83 0.69 0.71 0.77 0.79 0.74 0.7 0.77 0.87 0.9
Jan. Feb. Mar. Apr. May Jun. Jul. Aug. Sep. Oct. Nov. Dec.
0.85 0.8 0.75 0.7 0.65 0.6 0.55 0.5 0.45
b
gC m-2 d-1
GPP EC 1.25 1.36 1.51 2.21 2.68 2.56 3.02 2.45 1.81 1.45 1.14 1.09
GPP NIRv 1.77 1.54 1.37 1.88 2.25 2.36 2.61 2.15 1.74 1.81 1.85 1.98
GPP kNDVI 1.75 1.71 1.56 2.02 2.35 2.57 2.86 2.57 1.84 1.51 1.55 1.87
GPP REC 1.15 1.26 1.39 2.09 2.56 2.46 2.8 2.31 1.78 1.37 1.05 1
GPP VPM 1.2 1.29 1.45 2.05 2.27 2.58 2.93 2.59 1.89 1.42 1.06 1.11
GPP MODIS 1.31 1.38 1.54 2.27 2.88 2.92 3.59 2.99 2.12 1.51 1.2 1.16
GPP RF 0.89 1.02 1.22 1.84 2.21 2.23 2.7 2.24 1.54 1.1 0.86 0.85
GPP ERF 0.92 0.92 1.08 1.71 2.01 1.97 2.16 1.99 1.59 1.12 0.8 0.8
Jan. Feb. Mar. Apr. May Jun. Jul. Aug. Sep. Oct. Nov. Dec.
3.5 3 2.5 2 1.5 1
c
GPP EC 0.78 0.86 1.04 1.17 1.08 0.94 0.88 0.97 1.13 1.12 0.96 0.84
GPP NIRv 1.49 1.34 1.12 0.93 0.91 0.87 0.88 0.95 1.11 1.39 1.72 1.73
GPP kNDVI 1.55 1.4 1.11 0.86 0.89 0.9 0.9 0.92 0.99 1.18 1.5 1.69
GPP REC 0.8 0.84 1 1.17 1.12 0.97 0.91 0.98 1.13 1.1 0.96 0.86
GPP VPM 0.72 0.77 0.81 0.88 1 1.06 1.08 1.06 1 0.86 0.77 0.74
GPP MODIS 0.87 0.96 1.09 1.09 1.03 0.95 0.91 0.98 1.07 1.05 1.01 0.92
GPP RF 0.98 1.02 1.03 1.04 1.02 0.98 0.95 0.99 1.01 1.03 1.07 1.04
GPP ERF 0.98 0.97 0.96 0.96 1.01 0.97 0.96 1.01 1.08 1.08 1.07 1.03
Jan. Feb. Mar. Apr. May Jun. Jul. Aug. Sep. Oct. Nov. Dec.
1.5 1 0.5

Figure 3. Performance of the eight models in each month. a, b and c represent R^2, RMSE, and Sim/Obs respectively.

We further compared the performance of all models in different subvalues, including high value (GPP > 15 gC m^{-2} d^{-1}), median value (15 gC m^{-2} d^{-1} > GPP > 2 gC m^{-2} d^{-1}), low value (GPP < 2 gC m^{-2} d^{-1}). For extreme values, most models performed poorly (Figure 4), with R^2 for GPP estimate models falling below 0.3, and only GPP_{VPM} showing better performance in the high value. GPP_{ERF} demonstrated some improvement in both low and high values, with R^2 0.32 and 0.43, RMSE of 0.89 and 4.73 gC m^{-2} d^{-1}, and Sim/Obs closer to 1, respectively. In the median value, all models performed better, with no significant bias in the GPP estimate. The R^2 of GPP estimate models ranged from 0.44 to 0.68, and the RMSE remained between 1.82 and 2.54 gC m^{-2} d^{-1}. Further analysis was made at two typical sites, it was obvious that GPP_{EC}, GPP_{REC} and GPP_{MODIS} on CN-Qia exhibited obvious underestimation during the growing season (Figure S5). On CH_Lae, GPP_{kNDVI} and GPP_{VPM} were significantly overestimated (Figure S6). In contrast, at both sites, GPP_{ERF} was more consistent with observations~~, indicating that the superior performance of GPP~~~~ERF~~~~ was due to the corrections on the time series.~~.

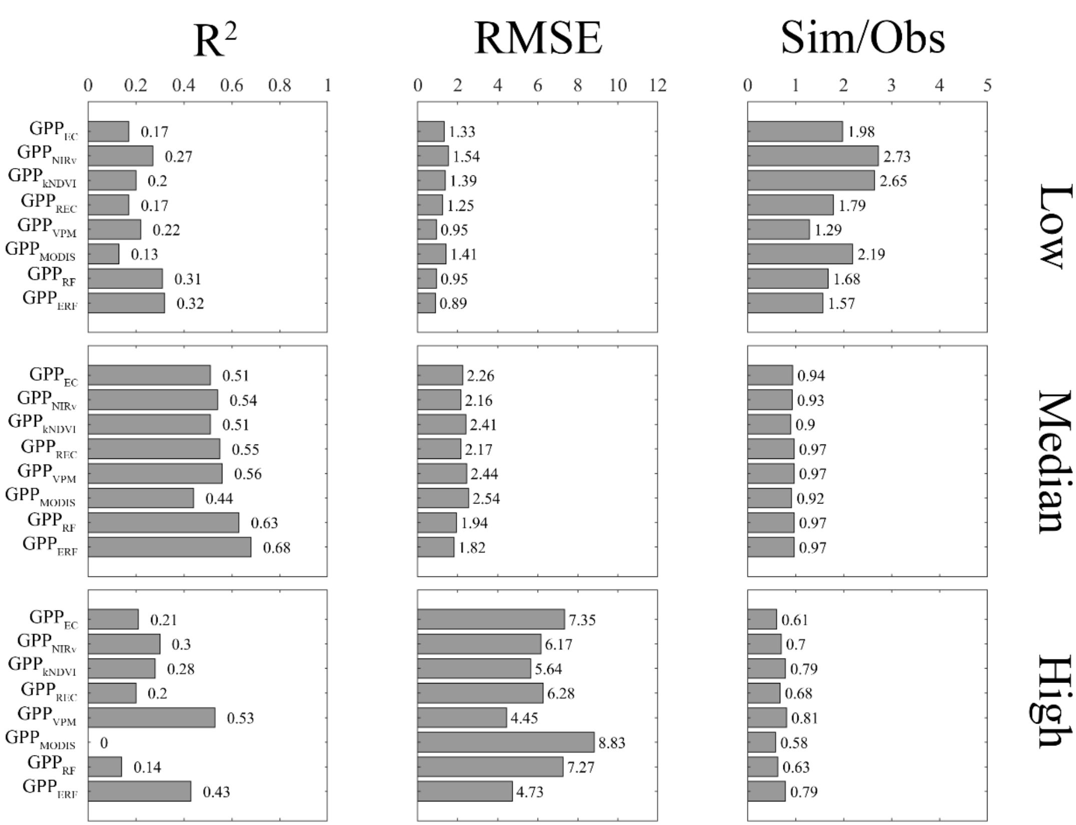

Figure 4. Performance of eight models in different subvalues.

3.3 Temporal and spatial characteristics of ~~ERF~~ ERF_GPP and its generalization evaluation

Figure 5a shows the spatial distribution of the multi-year average of ERF_GPP. The high values of GPP were mainly concentrated in tropical areas, exceeding 10 gC m^{-2} d^{-1}, and relatively high in southeastern North America, Europe and southern China, about 4-6 gC m^{-2} d^{-1}. From 2001-2022, China and India showed the fastest increase in GPP, mostly at 0.1 gC m^{-2} d^{-1} (Figure 5b), similar to a previous study that reported that China and India led the global greening (Chen et al., 2019). We further investigated the annual maximum GPP, as shown in Figure 5c, and the North American corn belt was the global leader in GPP at more than 15 gC m^{-2} d^{-1}, compared to only 10 gC m^{-2} d^{-1} in most tropical forests. In 2001-2022, the global GPP was 132.7 $\pm$2.8 PgC yr^{-1}, with an increasing trend of 0.42 PgC yr^{-2} (Figure 5d). The lowest value was 128.6 PgC yr^{-1} in 2001, and the highest value was 136.2 PgC yr^{-1} in 2020.

The results of the two uncertainty analyses consistently indicated that ERF_GPP exhibited higher uncertainty in tropical regions (Figures S7 and S8), and the uncertainty of ERF_GPP caused by the number of GPP observations was relatively small, the standard deviation of 100 simulations was about 0.3 gC m^{-2} d^{-1} in the tropics and lower in other regions, below 0.1 gC m^{-2} d^{-1}. In contrast, the uncertainty of ERF_GPP caused by the number of features was more pronounced, especially when fewer features were included in the model~~s~~. It is worth noting that when the number of features was five, the uncertainty was already substantially less, and the standard deviation was generally lower than 0.5 gC m^{-2} d^{-1}.

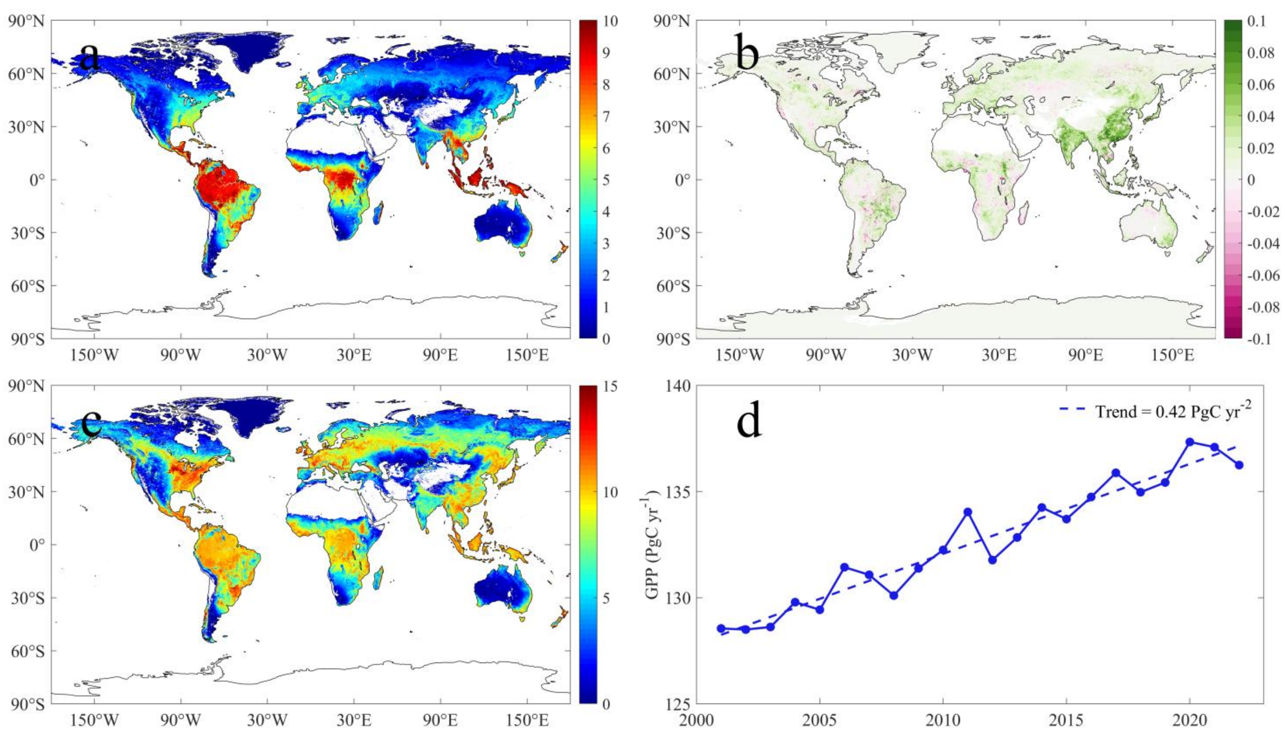

Figure 5. Spatial and temporal characteristics of ERF_GPP during 2001-2022.~~Spatial distribution and interannual changes of ERF_GPP during 2001-2022.~~ a represents the multi-year average, b represents the trend, c represents the multi-year average of the annual maximum~~the annual maximum~~, and d represents the interannual change of GPP.

As shown in Figure 6, ERF_GPP and other GPP datasets were validated using GPP observations from ChinaFlux. Among all models, ~~GPP$_{VPM}$~~ VPM demonstrated the best performance, with R^2 of 0.86 and RMSE of 1.34 gC m^{-2} d^{-1}. ERF_GPP also exhibited high generalization, with R^2 of 0.75, RMSE of 1.72 gC m^{-2} d^{-1}, there was no "high value underestimation and low value overestimation", which was comparable to the accuracy of BESS and GOSIF. However, the simulation accuracy of the other GPP datasets in Chinaflux was relatively poor, with the R^2 of NIRv being only 0.64, while FLUXCOM-ENS, FLUXCOM-RF, MODIS and Revised EC-LUE were significantly underestimated, with the Sim/Obs being only 0.71-0.89. In the validation of FLUXNET, the R^2 of FLUXCOM-ENS, MODIS, and Revised EC-LUE ranged from 0.57 to 0.67, and the RMSE ranged from 2.67 to 3.30 gC m^{-2} d^{-1}, and exhibited different degrees of underestimation (Figure S9). Other GPP datasets demonstrated similar performance, with ERF_GPP being the best (R^2 = 0.74, RMSE = 2.26 gC m^{-2} d^{-1}).

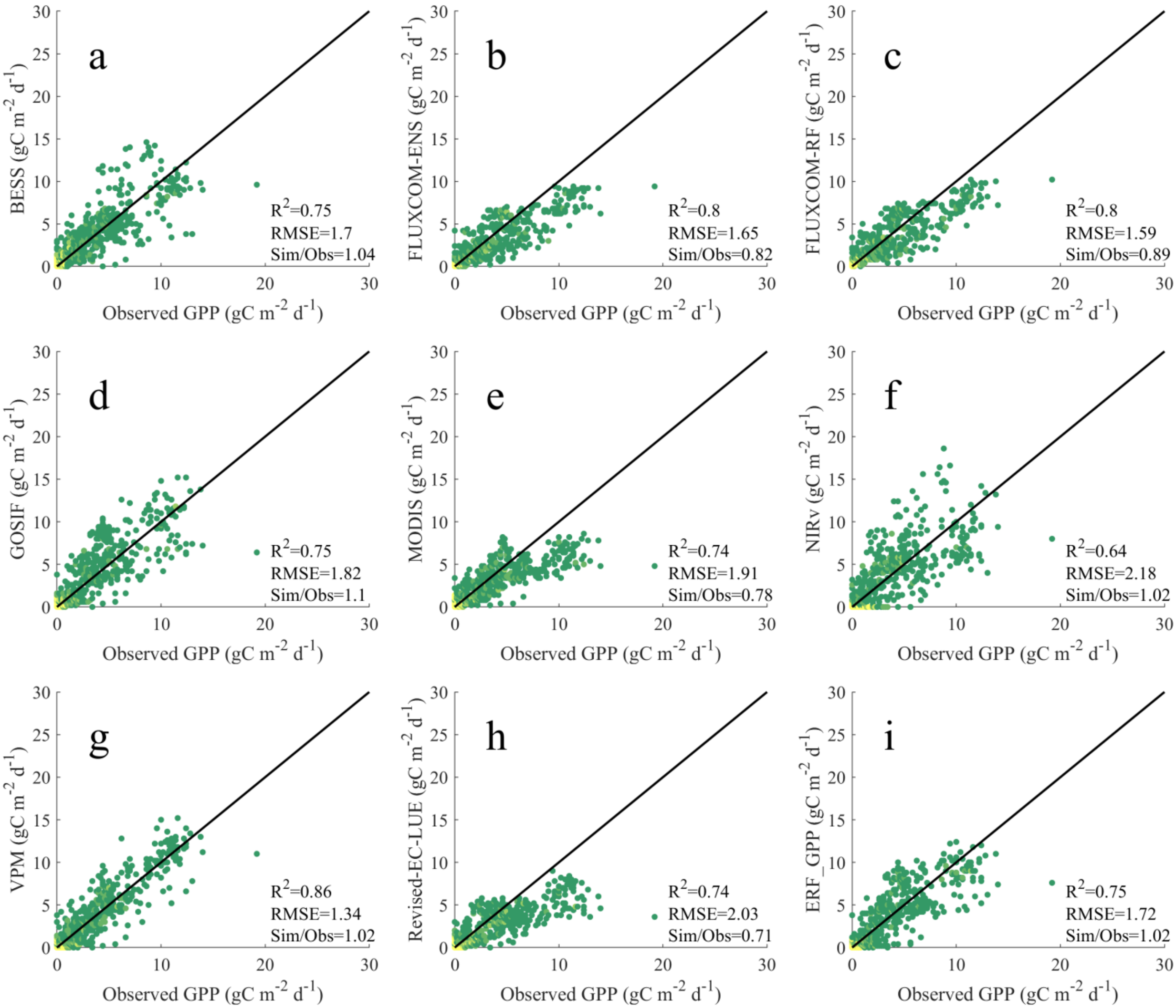

Figure 6. Comparison between the GPP datasets and the GPP observations from ChinaFlux. a-i represents BESS, FLUXCOM-ENS, FLUXCOM-RF, GOSIF, MODIS, NIRv, VPM, Revise-EC-LUE, ERF_GPP, respectively.

4 Discussion

4.1 Performance analysis of different models

After parameter calibration, both LUE and vegetation index models obtained reliable model accuracy. However, noticeable errors persist in different months and subvalues, indicating the prevalent phenomenon of "high value underestimation and low value overestimation" (Figures 1-4). In addition to MODIS, the GPP simulated by the other three LUE models is generally underestimated in winter (Figure 3), which may be caused by biases in the parameters used in meteorological constraints. In the expression form of the temperature constraint adopted by LUE models, the maximum temperature, minimum temperature and optimum temperature for limiting photosynthesis are all constants, however these values may not be fixed (Grossiord et al., 2020; Huang et al., 2019). A previous study has demonstrated that the GPP estimate could be effectively improved by using dynamic temperature parameters (Chang et al., 2021). Moreover, the form of meteorological constraint is also an important influencing factor. Compared with other LUE models, VPM does not use VPD constraints, but incorporates land surface water index from satellite observations as constraints (Xiao et al., 2004), which may be the reason why the model performs better than other models at high value (Figure 4). Conversely, the two vegetation index models overestimated GPP in winter, and even overestimated by 70% in December. The vegetation index model does not consider meteorological constraints that believe that all environmental impacts on vegetation have been included in the vegetation indices~~index~~ (kNDVI, NIRv). However, it is a fact that under high temperature or low radiation, the vegetation index may still maintain the appearance of high photosynthesis (greening), while in fact the GPP is low (Chen et al., 2024; Doughty et al., 2021; Yang et al., 2018). Furthermore, the relationship between these vegetation indices and GPP is not robust, and the vegetation indices based on reflectance may have hysteresis (Wang et al., 2022).

Compared to other GPP estimate models, the ERF model demonstrated better performance (R^2 = 851). Since there are no physical constraints, the machine learning model needs to find the relationship between explanatory variables and target variable from a large amount of training data (such as GPP=f (LAI, T, P, etc.)) (Guo et al., 2023; Jung et al., 2020). Therefore, the reliability of the model usually depends on the representativeness of the training data. For example, LAI can explain GPP to a large extent, while complex modeling relationships are still needed from LAI to GPP. The difference between the ERF model and the RF model lies in the explanatory variables. The ERF model uses multiple GPP simulations that are more representative and aligned with the target variable, thus making the GPP simulations more accurate. In other words, the ERF model does not need to take into account the uncertainties of the model structure (such as meteorological constraints) and model parameters (such as maximum light use efficiency), but rather focuses on the uncertainties inherent in the simulated GPP. To further clarify the impact of explanatory variables on the ERF model, we conducted a feature importance analysis (Figure S10). From an average of 200 times, the results of the ERF model did not depend on a single GPP simulation. Even GPP_{MODIS}, with the highest relative importance, accounted for no more than 25%, suggesting that the ERF model behaves more like a weighted average of multiple GPP simulations. In addition, it is important to emphasize that the accuracy of the ERF model is still robust even for GPP simulations of original parameters (Figure S4), which means that we can try to use this method to integrate the currently published GPP data sets to obtain a more accurate global GPP estimate.

It is worth noting that in the study of Tian et al. (2023), the ERF model was also used to improve the GPP estimate. Our study extends this work in several ways. Firstly, parameter calibration was carried out in our study so that the final validation results are comparable, that is, differences in model performance are mainly due to the uncertainty of the model structure. Secondly, our study focused on the phenomenon of "high value underestimation and low value overestimation" of GPP estimate models, with results indicating that the ERF model performed well across various vegetation types, months, and subvalues. Finally, we generated the ERF_GPP dataset and validated it on different observational datasets, further confirming the robustness of the ERF model in GPP estimate.

4.2 Robustness of ERF_GPP

Due to the inherent advantages of the RF method, the accuracy of the model was comparable to that of the ERF model, even if~~ we use~~ a very simple model that used longitude, latitude, month, and year as explanatory variables (Figure S11 a). However, the global GPP estimated by this model ~~is~~was not reliable (Figure S11 b). This means that it is unknown whether site-scale model~~s~~ can be fully applied to global GPP estimates. ERF model can overcome this limitation well. On the one hand, the explanatory variables used in the model are derived from GPP simulation in which contain a lot of remote sensing information, which can ensure that the global GPP estimated by the model is reliable. On the other hand, the second validation method also further shows that the ERF model has good generalization and has greater potential than other models in estimating global GPP.

Since the current GPP datasets are generated based on remote sensing data and FLUXNET GPP observations, there is a strong similarity in spatial distribution among all GPP datasets. Therefore, the validation of GPP observations independent of FLUXNET is crucial. Validation results from GPP observations of ChinaFlux indicated that ERF_GPP exhibited good generalization in China (R^2=0.75), which was slightly lower than the accuracy of 5-fold-cross-validation during modeling, possibly due to the mismatch between the 0.05 °GPP estimate and the footprint of the flux tower (Chu et al., 2021). In addition, the validation of FLUXNET further confirms the reliability of ERF_GPP. Overall, this is comparable to or slightly better than the simulation accuracy of current mainstream GPP datasets. We also observed a clear improvement in the spatial maximum value of ERF_GPP in some corn growing regions, such as the North American Corn Belt (Figure 5c), which is supported by previous studies showing that C4 crops have much higher GPP peaks than other vegetation types (Chen et al., 2011; Yuan et al., 2015).

Due to the increasing trend of drought, the constraining effect of water on vegetation is gradually increasing, and some studies have reported the decoupling phenomenon of LAI and GPP under some specific conditions (Hu et al., 2022; Jiao et al., 2021). However, in China and India with significant greening, GPP continues to increase in most datasets, and ERF_GPP supports this view. This phenomenon may be attributed to the low drought pressure on croplands in China and India due to irrigation, which poses less constraint on GPP (Ai et al., 2020; Ambika and Mishra, 2020). The global estimate of ERF_GPP is 132.7 ± 2.8 PgC yr^{-1}, which is close to estimates from most previous studies (Badgley et al., 2019; Wang et al., 2021). A study have suggested that global GPP may reach 150-175 PgC yr^{-1} (Welp et al., 2011), however, there is no further evidence to support this view.

ERF_GPP exhibited higher uncertainty in tropical regions, similar reports have been made in previously published GPP datasets (Badgley et al., 2019; Guo et al., 2023). The scarcity of flux observations in these regions (Pastorello et al., 2020), coupled with the well-known issue of cloud pollution and saturation in remote sensing data~~ in the tropics~~ (Badgley et al., 2019), exacerbates the uncertainty in GPP estimates for these regions. Therefore, in future studies, on the one hand, more flux observations in tropical regions are needed, and on the other hand, attempts can be made to combine optical and microwave data to improve GPP estimate.

4.3 Limitations and uncertainties

In this study, we improved GPP estimate based on the ERF model. Nonetheless, there are still some limitations and uncertainties due to the availability of data and methods. First, C4 crop distribution maps were used in our study to improve estimates of cropland GPP. However, ~~it is important to note that~~ this dataset only represents the spatial distribution of crops around the year 2000, which introduce uncertainty into GPP simulations of cropland in a few C3 and C4 alternating areas. Secondly, the ERF model considers six GPP simulations, and it is not clear whether adding more GPP simulations to the model can further improve the GPP estimate. Finally, our model did not consider the effect of soil moisture on GPP, and some previous studies have highlighted the importance of incorporating soil moisture in GPP estimates, especially for dry years (Stocker et al., 2018; Stocker et al., 2019).

5 Conclusion

In this study, we compared the performance of the ERF model with other GPP estimate models at the site scale, especially for the phenomenon of "high value underestimation and low value overestimation", and further developed the ERF_GPP dataset. Overall, GPP_{ERF} had higher model accuracy, explaining 85.1% of the monthly GPP variations, and demonstrated reliable accuracy in different months, vegetation types and subvalues. Over the period from 2001 to 2022, the global estimate of ERF_GPP was 132.7 ±2.8 PgC yr^{-1}, corresponding to an increasing trend of 0.42 PgC yr^{-2}. Validation results from ChinaFlux indicated that ERF_GPP had good generalization. For the current emerging GPP estimate models, the ERF model provides an alternative method that lead to better model accuracy.

Data and code availability

The ERF_GPP for 2001-2022 is available at https://doi.org/10.6084/m9.figshare.24417649 (Chen et al., 2023). The spatial resolution of ERF_GPP is 0.05° and the temporal resolution is monthly. Code is available from the author upon reasonable request.

Author contributions

X.C. and T.X.C. conceived the scientific ideas and designed this research framework. X.C. compiled the data, conducted analysis, prepared figures. X.C., T.X.C. and Y.F.C. wrote the manuscript. D.X.L., R.J.G., J.D., and S.J.Z. gave constructive suggestions for improving the manuscript.

Acknowledgments

This study was supported by the National Natural Science Foundation of China (No. 42130506, 42161144003 and 31570464) and the Postgraduate Research & Practice Innovation Program of Jiangsu Province (No. KYCX23_1322).

Declaration of interests

The authors have not disclosed any competing interests.

References

Ai, Z. et al., 2020. Variation of gross primary production, evapotranspiration and water use efficiency for global croplands. Agricultural and Forest Meteorology, 287.

Ambika, A.K. and Mishra, V., 2020. Substantial decline in atmospheric aridity due to irrigation in India. Environmental Research Letters, 15(12).

Anav, A. et al., 2015. Spatiotemporal patterns of terrestrial gross primary production: A review. Reviews of Geophysics, 53(3): 785-818.

Badgley, G., Anderegg, L.D., Berry, J.A. and Field, C.B., 2019. Terrestrial gross primary production: Using NIRV to scale from site to globe. Global change biology, 25(11): 3731-3740.

Badgley, G., Field, C.B. and Berry, J.A., 2017. Canopy near-infrared reflectance and terrestrial photosynthesis. Science advances, 3(3): e1602244.

Bai, Y. et al., 2021. On the use of machine learning based ensemble approaches to improve evapotranspiration estimates from croplands across a wide environmental gradient. Agricultural and Forest Meteorology, 298: 108308.

Belgiu, M. and Drăguţ, L., 2016. Random forest in remote sensing: A review of applications and future directions. ISPRS journal of photogrammetry and remote sensing, 114: 24-31.

Camps-Valls, G. et al., 2021. A unified vegetation index for quantifying the terrestrial biosphere. Science Advances, 7(9): eabc7447.

Chang, Q. et al., 2021. Assessing variability of optimum air temperature for photosynthesis across site-years, sites and biomes and their effects on photosynthesis estimation. Agricultural and Forest Meteorology, 298.

Chen, C. et al., 2019. China and India lead in greening of the world through land-use management. Nature Sustainability, 2(2): 122-129.

Chen, T., Van Der Werf, G., Gobron, N., Moors, E. and Dolman, A., 2014. Global cropland monthly gross primary production in the year 2000. Biogeosciences, 11(14): 3871-3880.

Chen, T., van der Werf, G.R., Dolman, A.J. and Groenendijk, M., 2011. Evaluation of cropland maximum light use efficiency using eddy flux measurements in North America and Europe. Geophysical Research Letters, 38.

Chen, X. et al., 2024. Vegetation Index‐Based Models Without Meteorological Constraints Underestimate the Impact of Drought on Gross Primary Productivity. Journal of Geophysical Research: Biogeosciences, 129(1): e2023JG007499.

Chen, Y., Yuan, H., Yang, Y. and Sun, R., 2020. Sub-daily soil moisture estimate using dynamic Bayesian model averaging. Journal of Hydrology, 590: 125445.

Chu, H. et al., 2021. Representativeness of Eddy-Covariance flux footprints for areas surrounding AmeriFlux sites. Agricultural and Forest Meteorology, 301: 108350.

Dechant, B. et al., 2022. NIRVP: A robust structural proxy for sun-induced chlorophyll fluorescence and photosynthesis across scales. Remote Sensing of Environment, 268: 112763.

Dechant, B. et al., 2020. Canopy structure explains the relationship between photosynthesis and sun-induced chlorophyll fluorescence in crops. Remote Sensing of Environment, 241: 111733.

Doughty, R. et al., 2021. Small anomalies in dry-season greenness and chlorophyll fluorescence for Amazon moist tropical forests during El Nino and La Nina. Remote Sensing of Environment, 253.

Grossiord, C. et al., 2020. Plant responses to rising vapor pressure deficit. New Phytologist, 226(6): 1550-1566.

Guo, R. et al., 2023. Estimating Global GPP From the Plant Functional Type Perspective Using a Machine Learning Approach. Journal of Geophysical Research-Biogeosciences, 128(4).

Hersbach, H. et al., 2020. The ERA5 global reanalysis. Quarterly Journal of the Royal Meteorological Society, 146(730): 1999-2049.

Hu, Z. et al., 2022. Decoupling of greenness and gross primary productivity as aridity decreases. Remote Sensing of Environment, 279: 113120.

Huang, M. et al., 2019. Air temperature optima of vegetation productivity across global biomes. Nature ecology & evolution, 3(5): 772-779.

Jiao, W. et al., 2021. Observed increasing water constraint on vegetation growth over the last three decades. Nature Communications, 12(1).

Jung, M. et al., 2020. Scaling carbon fluxes from eddy covariance sites to globe: synthesis and evaluation of the FLUXCOM approach. Biogeosciences, 17(5): 1343-1365.

Li, B. et al., 2023. BESSv2.0: A satellite-based and coupled-process model for quantifying long-term global land-atmosphere fluxes. Remote Sensing of Environment, 295.

Li, X. and Xiao, J., 2019. A Global, 0.05-Degree Product of Solar-Induced Chlorophyll Fluorescence Derived from OCO-2, MODIS, and Reanalysis Data. Remote Sensing, 11(5).

Monfreda, C., Ramankutty, N. and Foley, J.A., 2008. Farming the planet: 2. Geographic distribution of crop areas, yields, physiological types, and net primary production in the year 2000. Global Biogeochemical Cycles, 22(1).

Pastorello, G. et al., 2020. The FLUXNET2015 dataset and the ONEFlux processing pipeline for eddy covariance data. Scientific data, 7(1): 1-27.

Pei, Y. et al., 2022. Evolution of light use efficiency models: Improvement, uncertainties, and implications. Agricultural and Forest Meteorology, 317: 108905.

Ruehr, S. et al., 2023. Evidence and attribution of the enhanced land carbon sink. Nature Reviews Earth & Environment, 4(8): 518-534.

Running, S.W. et al., 2004. A continuous satellite-derived measure of global terrestrial primary production. Bioscience, 54(6): 547-560.

Ryu, Y., Berry, J.A. and Baldocchi, D.D., 2019. What is global photosynthesis? History, uncertainties and opportunities. Remote sensing of environment, 223: 95-114.

Stocker, B.D. et al., 2018. Quantifying soil moisture impacts on light use efficiency across biomes. New Phytologist, 218(4): 1430-1449.

Stocker, B.D. et al., 2019. Drought impacts on terrestrial primary production underestimated by satellite monitoring. Nature Geoscience, 12(4): 264-+.

Tian, Z. et al., 2023. Fusion of Multiple Models for Improving Gross Primary Production Estimation With Eddy Covariance Data Based on Machine Learning. Journal of Geophysical Research: Biogeosciences, 128(3): e2022JG007122.

Wang, J. et al., 2017. Decreasing net primary production due to drought and slight decreases in solar radiation in China from 2000 to 2012. Journal of Geophysical Research: Biogeosciences, 122(1): 261-278.

Wang, S., Zhang, Y., Ju, W., Qiu, B. and Zhang, Z., 2021. Tracking the seasonal and inter-annual variations of global gross primary production during last four decades using satellite near-infrared reflectance data. Science of the Total Environment, 755: 142569.

Wang, X. et al., 2022. Satellite solar-induced chlorophyll fluorescence and near-infrared reflectance capture complementary aspects of dryland vegetation productivity dynamics. Remote Sensing of Environment, 270: 112858.

Welp, L.R. et al., 2011. Interannual variability in the oxygen isotopes of atmospheric CO₂ driven by El Nino. Nature, 477(7366): 579-582.

Xiao, J. et al., 2019. Remote sensing of the terrestrial carbon cycle: A review of advances over 50 years. Remote Sensing of Environment, 233: 111383.

Xiao, X. et al., 2004. Modeling gross primary production of temperate deciduous broadleaf forest using satellite images and climate data. Remote sensing of environment, 91(2): 256-270.

Xu, T., White, L., Hui, D. and Luo, Y., 2006. Probabilistic inversion of a terrestrial ecosystem model: Analysis of uncertainty in parameter estimation and model prediction. Global Biogeochemical Cycles, 20(2).
Yang, J. et al., 2018. Amazon drought and forest response: Largely reduced forest photosynthesis but slightly increased canopy greenness during the extreme drought of 2015/2016. Global Change Biology, 24(5): 1919-1934.
Yao, Y. et al., 2017. Improving global terrestrial evapotranspiration estimation using support vector machine by integrating three process-based algorithms. Agricultural and Forest Meteorology, 242: 55-74.
Yao, Y. et al., 2014. Bayesian multimodel estimation of global terrestrial latent heat flux from eddy covariance, meteorological, and satellite observations. Journal of Geophysical Research: Atmospheres, 119(8): 4521-4545.
Yuan, W. et al., 2015. Uncertainty in simulating gross primary production of cropland ecosystem from satellite-based models. Agricultural and Forest Meteorology, 207: 48-57.
Yuan, W. et al., 2014. Global comparison of light use efficiency models for simulating terrestrial vegetation gross primary production based on the LaThuile database. Agricultural and Forest Meteorology, 192: 108-120.
Yuan, W. et al., 2007. Deriving a light use efficiency model from eddy covariance flux data for predicting daily gross primary production across biomes. Agricultural and Forest Meteorology, 143(3-4): 189-207.
Yuan, W. et al., 2019. Increased atmospheric vapor pressure deficit reduces global vegetation growth. Science advances, 5(8): eaax1396.
Zhang, Y. et al., 2017. A global moderate resolution dataset of gross primary production of vegetation for 2000–2016. Scientific data, 4(1): 1-13.
Zheng, Y. et al., 2020. Improved estimate of global gross primary production for reproducing its long-term variation, 1982–2017. Earth System Science Data, 12(4): 2725-2746.